Microporous and Mesoporous Materials 130 (2010) 26–31

Contents lists available at ScienceDirect

Microporous and Mesoporous Materials

journal homepage: www.elsevier.com/locate/micromeso

# Magnetic 3-D ordered macroporous silica templated from binary colloidal crystals and its application for effective removal of microcystin

Jia Liu, Yue Cai, Yonghui Deng *, Zhenkun Sun, Dong Gu, Bo Tu, Dongyuan Zhao *

*Department of Chemistry, Shanghai Key Laboratory of Molecular Catalysis and Innovative Materials, Advanced Materials Laboratory, Fudan University, Shanghai 200433, PR China*

ARTICLE INFO

*Article history:*
Received 17 August 2009
Received in revised form 30 September 2009
Accepted 9 October 2009
Available online 8 November 2009

*Keywords:*
Macroporous materials
Colloidal crystal
Magnetic property
Microcystin

ABSTRACT

Magnetic 3-D ordered macroporous siliceous materials were conveniently fabricated by combination of a simple co-sedimentation of binary colloidal system of PMMA spheres and magnetite nanoparticles and the infiltration of silica precursors. The SEM and TEM observations indicate that the obtained magnetic 3-D ordered macroporous silica materials have face-centered cubic (*fcc*) packing structure with ordered macropore of ~200 nm and interconnected windows of about 50 nm. Magnetic property characterization shows that the magnetic 3-D ordered macroporous silica materials possess high magnetization (19.2 emu/g) and superparamagentism. By utilization of their ordered macroporous structure with large entrances and good affinity for biomacromolecules as well as high magnetization, a fast and efficient removal of microcystin in water with high removal efficiency (>93%) and removal capacity (3.3 ng MC/mg) was achieved with the help of an applied magnetic field.



## 1. Introduction

Ordered porous materials with tailorable pore size and functionalities have recently attracted great attention for their wide potential applications in photonic crystals, bio-separation, catalysis, drug delivery and electrochemical cells [1–3]. Particularly, ordered macroporous materials, due to periodically large nanostructure, tunable pore size, large entrance and easily functionalizable surface show great promise in various applications involving large biomolecules [4–7]. Many methods have been reported to fabricate ordered macroporous materials, including soft lithograph, emulsion templating synthesis and so on [8,9]. One of the most common approaches is the hard-templating process with colloidal crystals of monodisperse spheres as the sacrificial templates [10–12]. The guest molecules can be introduced into the interstitial voids of the colloidal crystals through different strategies, such as solution or melt infiltration, sol–gel chemistry, *in situ* polymerization, electrodeposition and chemical vapor deposition (CVD) [12,13]. The subsequent removal of the templates through thermal or chemical etching leads to ordered macroporous materials. In the past decades, ordered macroporous materials with various compositions have been fabricated, including ceramics oxides, metals, polymers, semiconductors [14–18].

Magnetic nanomaterials, due to their unique magnetic behavior, have recently attracted increasing attention for their potential applications in biomedicine, separation and enrichment, magnetic nanodevice [19–21]. Functionalization of the ordered macroporous materials with magnetic property is of great interest to their applications, because the additional magnetic property can greatly facilitate the manipulation of macroporous materials. By using colloidal crystal templates, Eagleton and Searson synthesized magnetic ordered macroporous nickels by an electrodeposition [22]. Stein and co-workers synthesized magnetic ordered macroporous nickels, cobalts and their oxides [23]. Galloro et al. synthesized ordered macroporous maghemites ($\gamma$–$Fe_2O_3$) through an infiltrating colloidal crystal with polyferrocenylsilane followed by calcination to remove the template [24]. The above mentioned magnetic macroporous materials are difficult to further modify by functional groups, which may limit their applications. Usually, for bio-related applications, the magnetic ordered macroporous materials should have easily functionalizable surface, high magnetic responsiveness and good bio-affinity, however, to our best knowledge, most of the reported magnetic ordered macroporous materials fail to meet these requirements.

Herein, we report a synthesis of magnetic 3-D ordered macroporous siliceous materials templated from binary colloidal crystals by combination of a simple co-sedimentation of binary colloidal system of PMMA spheres and magnetite nanoparticles and the infiltration of silica precursors. The obtained magnetic 3-D ordered macroporous silica materials possess face-centered cubic (*fcc*) packing structure with ordered macropore of ~200 nm, interconnected windows of about 50 nm, high magnetization (19.2 emu/g) and superparamagentism. Due to their ordered macroporous structure with large entrances and good affinity for biomacromol-

* Corresponding authors. Tel.: +86 21 51630205; fax: +86 21 65641740.
*E-mail addresses:* yhdeng@fudan.edu.cn (Y. Deng), dyzhao@fudan.edu.cn (D. Zhao).

1387-1811/$ - see front matter © 2009 Elsevier Inc. All rights reserved.
doi:10.1016/j.micromeso.2009.10.008

ecules as well as high magnetization, they show a fast and efficient removal of microcystin in water with high removal efficiency (>93%) and removal capacity (3.3 ng MC/mg) with the help of an applied magnetic field.

## 2. Experimental

### 2.1. Chemicals

Monodisperse PMMA microspheres were prepared *via* a surfactant-free emulsion polymerization process by using potassium persulfate as the initiator according to previous report [25]. The microspheres were negatively charged (with $SO_4^{2-}$ groups on the surface) which were dispersed into the deionized water producing concentration of 9.1 wt.%. Tetraethyl orthosilicate (TEOS), ethanol, aqueous ammonia, ferrous chloride, trisodium citrate and sodium nitrite were analytical reagents and purchased from Shanghai Chemical Company. All chemicals were used as received without further purification. Deionized water was used in all experiments. For microcystin removal experiments, α-cyano-4-hydroxycinnamic acid (CHCA), acetonitrile (ACN) and trifluoroacetic acid (TFA) were purchased from Merck (Darmstadt, Germany) and aqueous solutions were prepared using Milli-Q water by Milli-Q system (Millipore, Bedford, MA). Microcystin-LR (purity ⩾ 96%) was purchased from Alexis Corporation (San Diego, USA).

### 2.2. Synthesis of magnetite nanoparticles

Magnetite nanoparticles were synthesized by redox reaction [26] between nitrite and ferrous ($Fe^{2+}$) salts in a basic aqueous solution at 25 °C. Typically, 5.8 mmol of sodium nitrite was added to an aqueous solution containing 13 mmol $FeCl_2{\cdot}4H_2O$, 20 mL of HCl (2.0 M) and 800 mL of water. After stirring for 5 min, 80 mL of concentrated ammonia aqueous solution (28 wt.%) was added to the solution, resulting in a black dispersion. After vigorous stirring for 0.5 h, the magnetite nanoparticles were separated by using a magnet (1000 Oe) and washed with deionized water. To enhance the colloidal dispersibility, the magnetite nanoparticles were treated in 50 mL of nitric acid solution (2.0 M) for 5 min and then separated from the dispersion for redispersion in 100 mL of trisodium citrate aqueous solution (0.5 M) with ultrasonic treatment. After vibration for 10 min, the magnetite nanoparticles were separated and redispersed in deionized water to obtain stable magnetic fluid with solid content of 2.0 wt.%.

### 2.3. Synthesis of macroporous silica–magnetite composites

The magnetic fluid (20 g, 2 wt.%) and aqueous dispersion of PMMA colloids with the size of 250 nm (5.0 g, 5 wt.%) were mixed in an glass under ultrasonication. Then, the obtained solution was placed in an oven at 70 °C for fast solvent evaporation for 5–8 h, and the gray PMMA-magnetite binary colloidal crystals were obtained. After further sintering treatment at 90 °C for 24 h, the colloidal crystals were soaked in a silica precursor ethanol solution for 3 h at 25 °C, herein, the silica precursor was pre-hydrolyzed by mixing 0.9 g of TEOS, 2.0 mL of $H_2O$, 10 mL of ethanol and 0.1 mL of HCl (2.0 M). Afterward, the silica impregnated colloidal crystals were withdrawn from the solution and allowed to exposure to air for evaporation of ethanol and hydrolysis of the silica precursor. The above impregnation procedure was repeated for 3 times to ensure the fully filling of all the interstitial voids in the binary colloid crystals by the silica species. Finally, the composites were pyrolyzed in a tube furnace at 400 °C for 5 h in $N_2$ with a heating rate of 2 °C $min^{-1}$.

### 2.4. Removal of microcystins (MCs)

A certain volume of aqueous suspension of ordered macroporous magnetic-silica composites (100 mg $L^{-1}$) was added into a comparison tube, and the water was decanted with the help of a magnet. Then the magnetic material was redispersed with 200 μL of MC-LR (10 μg/L). The solution containing the magnetic-silica composites and MC-LR was shaken at 25 °C for 10 min. Subsequently, the magnetic composites with absorbed MC-LR were separated from the solution with a magnet, and 1.0 μL of the supernatant liquor was deposited on the plate, and then 5.0 μL of a mixture of 0.5 mg $mL^{-1}$ CHCA (in 50% (v/v) acetonitrile and 0.1% (v/v) TFA aqueous solution) was introduced. After dried, the samples were applied for matrix-assisted laser desorption/ionization time-of-flight mass spectrometry (MALDI-TOF MS) analysis.

### 2.5. Characterizations and measurements

Scanning electron microscopy (SEM) images were recorded on a Philips XL30 electron microscope (Netherlands) operating at 20 kV. A thin gold film was sputtered on the sample before the characterization. Transmission electron microscopy (TEM) images were taken with a JEOL 2011 microscope (Japan) operating at 200 kV. For the TEM measurements, the samples were dispersed in ethanol and then dried on a holey carbon film Cu grid. The wide-angle X-ray diffraction (XRD) patterns were performed on a German Bruker D4 X-ray diffractometer (Germany) with Ni-filtered Cu Kα radiation (40 kV, 40 mA). Fourier-transform infrared (FT-IR) spectra were collected on a Nicolet Fourier spectrophotometer (USA) using KBr pellets. Magnetic characterization was carried out on a superconducting quantum interference device (SQUID) magnetometry. MALDI-TOF MS experiments were performed in positive ion mode on a 4700 Proteomics Analyzer (Applied Biosystems, USA) with the Nd-YAG laser at 355 nm, a repetition rate of 200 Hz and an acceleration voltage of 20 kV. Analysis of MC was performed in the reflector TOF detection mode.

## 3. Results and discussion

The fabrication of magnetic 3-D macroporous silica materials is illustrated in Scheme 1. Firstly, a homogeneous and stable aqueous dispersion containing monodisperse negatively charged poly(methylmethacrylate) (PMMA) colloids and $Fe_3O_4$ nanoparticles stabilized with citrate groups was subject to heating at 70 °C for the binary assembly of PMMA and $Fe_3O_4$ colloids. Secondly, the resulting composite crystals were heated at 90 °C and then impregnated with a pre-hydrolyzed tetraethyl orthosilicate (TEOS) ethanol solu-

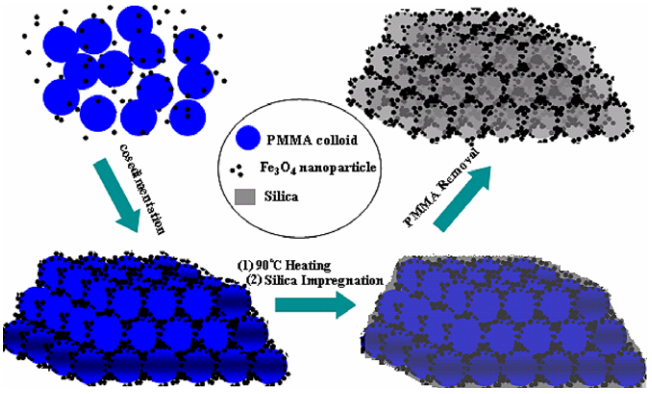


**Scheme 1.** The synthesis procedure for the magnetic 3-D ordered macroporous silica materials.

tion followed with drying in air to completely fill the voids in the binary colloid crystals with silica species. Finally, calcination in $N_2$ to remove the PMMA template leads to magnetic ordered macroporous silica.

The monodisperse PMMA colloids were synthesized through the soap-free emulsion polymerization method. The scanning electron microscopy (SEM) image shows that the PMMA colloids have a uniform size of 250 nm with a deviation <5% (Fig. 1a). The magnetite nanoparticles stabilized with citrate groups were prepared by a simple redox method (Fig. 2). Due to the stabilization effect of citrate groups, the obtained magnetite nanoparticles can be well dispersed in aqueous solution (Fig. 2, inset). TEM observation indicates they have small particle size of about 6–10 nm (Fig. 2). After the co-sedimentation and impregnation with silica oligomer species, the obtained composite colloidal crystals (Fig. 1b) possess typical face-centered cubic (*fcc*) packing structure with (1 1 1) plane parallel to the substrate, and the interstitial voids were found to be fully filled (Fig. 1b, inset). It indicates that the silica is successfully introduced into the colloidal crystals and solidified the ordered macrostructure. After calcination in $N_2$, highly ordered 3-D macroporous structure was obtained (Fig. 1c). The macropore size measured by SEM images is about 200 nm, less than the diameter (250 nm) of the PMMA colloid templates, suggesting that a considerable structure shrinkage occurs during the calcination process. The windows of the macropores are clearly visible and the diameter is calculated to be about 50 nm (Fig. 1d). The large window is originated from the large contact surface between the neighboring PMMA colloids formed by slightly melting the colloids during heating at near their glass transition temperature ($T_g$) of 90 °C prior to the silica impregnation [27–29]. The large window size is beneficial to the fast mass transportation for applications involving macromoelcules. Additionally, as shown in the SEM image (Fig. 1d), the obtained macroporous material has a rough framework, implying that the $Fe_3O_4$ nanoparticles are incorporated in the silica matrix.

The removal of PMMA template was verified by fourier-transform infrared (FT-IR) spectra. The absorption bands of the $Fe_3O_4$—$SiO_2$—PMMA composites at 2800–3000 and 1730 $cm^{-1}$ are attributed to —$CH_2$ and —C=O of PMMA, respectively (Curve b, Fig. 3). The peaks at 1090 and 560 $cm^{-1}$ are from the Si—O—Si of silica and Fe—O of $Fe_3O_4$ particles, respectively. After calcination, only absorption peaks for $Fe_3O_4$ and silica are observed in the magnetic macroporous silica (Curve b, Fig. 3), suggesting that PMMA templates can be fully decomposed in $N_2$ at 400 °C [30].

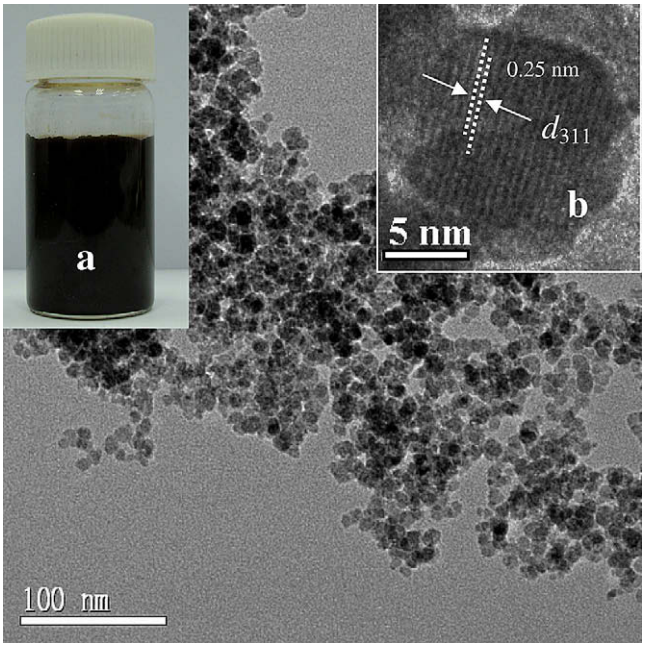


**Fig. 2.** TEM of magnetite nanoparticles prepared at room temperature of 25 °C. The inset (a) shows the photograph of the aqueous dispersion of the magnetite nanoparticles. The inset (b) is the high-resolution TEM image of a single magnetite nanoparticle.

The transmission electron microscopy (TEM) image (Fig. 4a) of the obtained magnetite-silica composites shows highly ordered

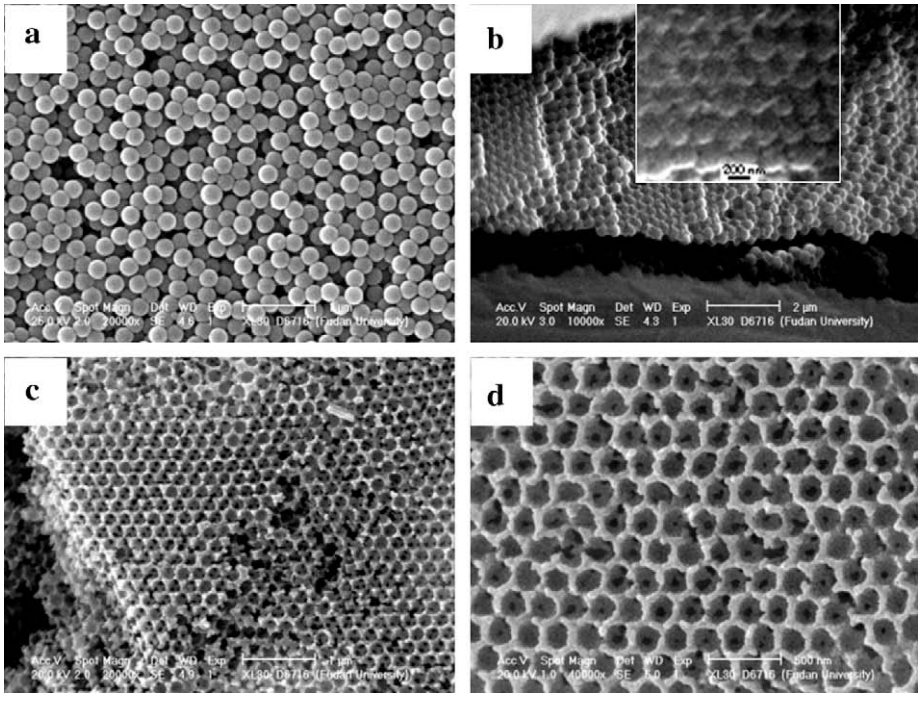


**Fig. 1.** SEM images of (a) PMMA colloids, (b) silica impregnated PMMA—$Fe_3O_4$ colloidal crystals, and (c, d) magnetic 3-D ordered porous silica.

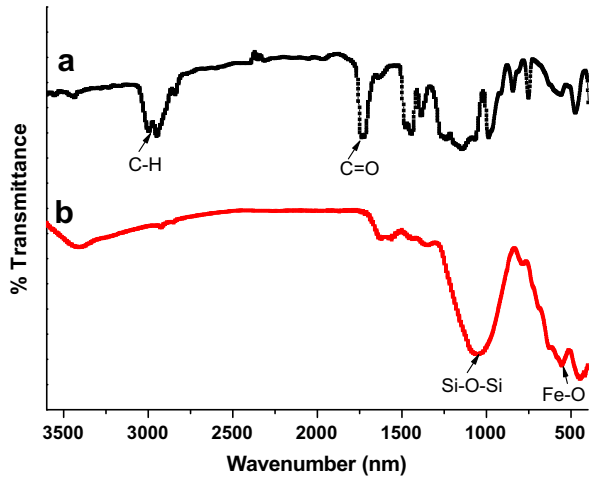


**Fig. 3.** FT-IR spectra of (a) as-made magnetite-silica-PMMA composite colloidal crystals and (b) 3-D ordered macroporous magnetic-silica composites after calcination in $N_2$ at 400 °C for 5 h.

macropore arrays viewed along the [2 1 1] direction of an *fcc* lattice, further confirming the replication of ordered macrostructure of the binary colloidal crystals. The TEM image with large magnification (Fig. 4b) clearly shows that the magnetite nanoparticles with diameter of 6–10 nm are homogeneously distributed in the silica matrix around the macropores. The silica component of the frameworks is very important. Firstly, it serves as "glue" for binding the magnetite nanoparticles and supporting the 3-D ordered macrostructure during the impregnation and calcination process. Secondly, it acts as protective coating for the nanoparticles to prevent them from being etched in practical applications. Thirdly, it provides silica-like surface for binding the objects or for further surface functionalization with organic groups. The HRTEM images clearly reveal that the magnetite nanoparticles are well crystallized (Fig. 4c). Selected area electron diffraction (SAED) patterns (Fig. 4d) show spotty diffraction cycles assigned to magnetite, indicating a polycrystalline feature.

X-ray diffraction (XRD) patterns (Fig. 5) of the ordered macroporous magnetic silicas show characteristic diffraction peaks of magnetite, suggesting that the $Fe_3O_4$ nanoparticles are well retained in the silica matrix. Compared to pure magnetite nanoparticles (Curve a in Fig. 5), the diffraction peaks of magnetic 3-D ordered macroporous silica are somewhat wider, which is probably caused by the coating of silica (Curve b in Fig. 5). Magnetic characterization with a superconducting quantum interference device (SQUID) magnetometer at 300 K indicates that the magnetite nanoparticles and the 3-D macroporous silica composites have magnetization saturation values of 49.0 and 19.2 emu/g, respectively (Fig. 6), indicating a high magnetization. Accordingly, the magnetite content in the macroporous composites is calculated to be as high as 39 wt.%, indicating a high magnetization. Additionally, no remanence is detected for both of them, indicating a superparamagnetism feature due to the nanosized $Fe_3O_4$. As a result of good magnetic property, the magnetic 3-D ordered macroporous silica composites suspended in water (0.05 g/mL) can be quickly separated from its dispersion with a magnet (1000 Oe). These re-

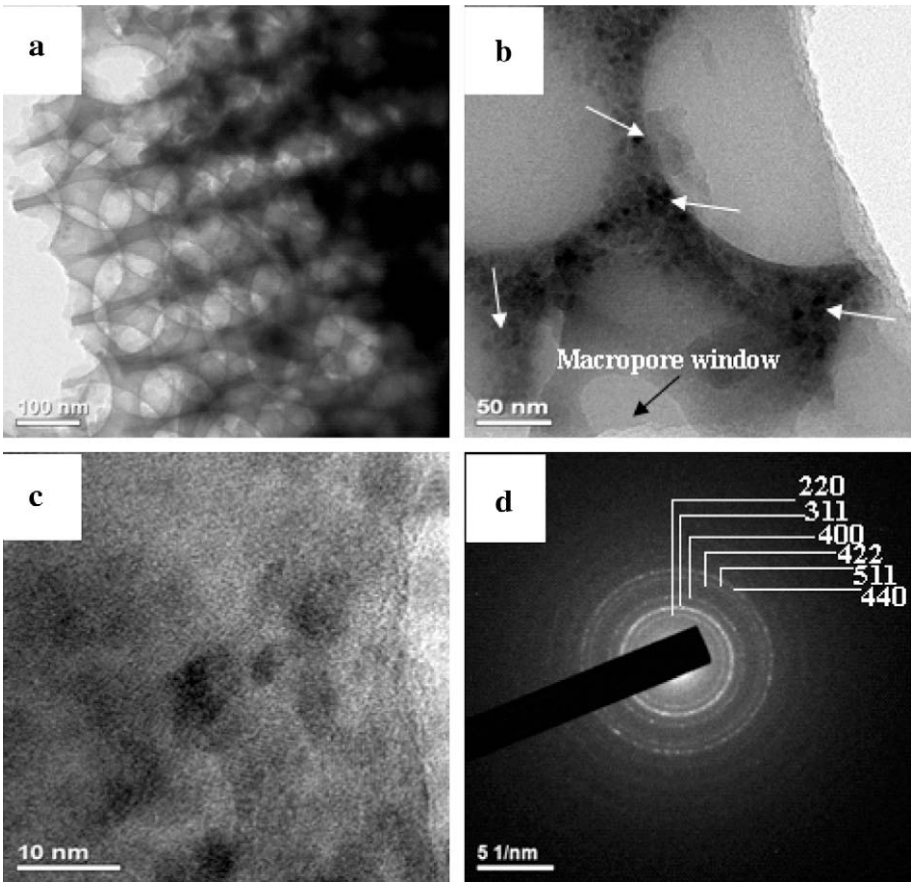


**Fig. 4.** TEM (a and b) and HRTEM (c) images of magnetic macroporous silica materials, and SAED pattern of the macroporous frameworks. The white arrows indicate the location of magnetic nanoparticles.

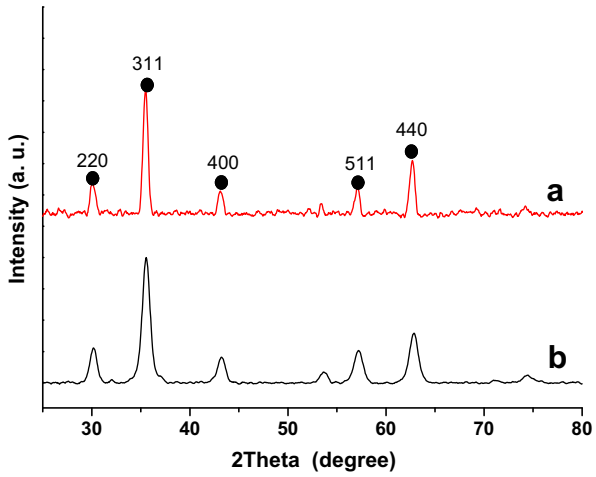


**Fig. 5.** Wide-angle XRD patterns of (a) magnetite nanoparticles prepared by redox reaction at 25 °C, and (b) the obtained 3-D ordered macroporous magnetic-silica composite materials.

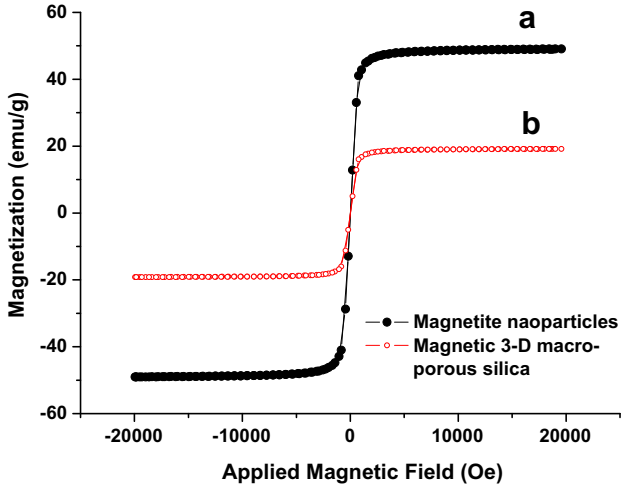


**Fig. 6.** The magnetic hysteresis loops of (a) magnetite nanoparticles and (b) the 3-D ordered macroporous magnetic-silica composite materials recorded at 300 K.

sults indicate that the magnetic macroporous silica composites possess excellent magnetic responsivity. Notably, other silica precursor, such as 3-aminopropyltrimethoxysilane, can be employed produce magnetic macroporous silica with organic functional groups.

Microcystins (MCs), a family of cyclic heptapeptide toxins with large molecular dimension (2–3 nm) (Fig. 7), are produced by cyanobacteria bloom occurred widely in many eutrophic water. MCs threaten seriously the human health for their wide distribution in nature water and their potent tumor promoting activity through the inhibition of protein phosphatases. The MC content in the Taihu Lake water, the third fresh lake of China, is measured to be about 10 μg/L [31]. Various methods have therefore been proposed for removal of MCs in water [32,33]. The conventional coagulation and sand filtration can eliminate particulate cyanobacterial cells but fail to remove the highly water-dissolvable MCs (solubility > 1 g/L). Activated carbon can adsorb MCs, but it requires large amount of the sorbents because of the deficiency of accessible large mesopores for large molecular MCs. In this study, by using our macroporous magnetic-silica composites as an absorbent, we explored their application for the

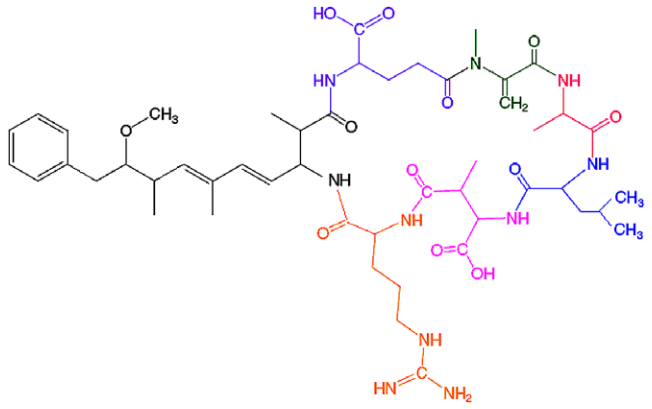


**Fig. 7.** Chemical structure of microcystins (MC-LR).

removal of MC-LR in water. The removal efficiency was analyzed by matrix-assisted laser desorption/ionization time-of-flight mass spectrometry (MALDI-TOF MS). To investigate the influence of the addition amount of the magnetic materials on the residual quantity of MC-LR, various amounts of the magnetic materials ranging from 0 to 1.0 mg were used for MC-LR solution (200 μL, 10 μg/L for each batch) (Fig. 8). MALDI-TOF measurements show that only small addition (0.1 mg) of magnetic materials can reach a high removal efficiency (~93%) with a residual MC-LR quantity of ~0.7 μg/L, meeting the guideline for drinking-water standard (1 μg/L) proposed by WHO [34]. As the addition amount increases, the MC-LR remained in the supernate significantly decreased. Fig. 9 shows the MS spectra of MC-LR solution (200 μL, 10 μg/L) before and after treated by 0.6 mg of magnetic 3-D macroporous silica, from which one can clearly find that after treatment with magnetic-silica materials, almost no signal was detected at around 990 m/z, characteristic for MC-LR, indicating a high adsorption ability (3.3 ng MC/mg magnetic absorbent). Additionally, repeated experiments show that our magnetic 3-D macroporous silica can be well recycled without significant loss of removal efficiency.

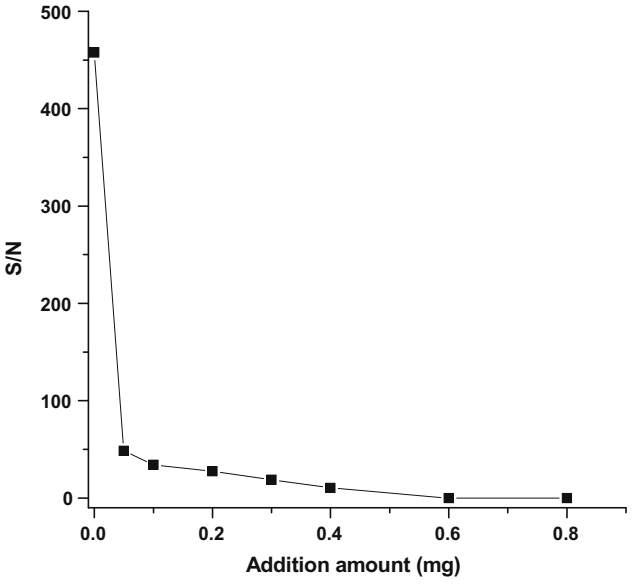


**Fig. 8.** The removal efficiency functioned with the amount of the macroporous magnetic-silica composites. For each adsorption, 200 μL of aqueous solutions of MC-LR (10 μg/L$^{-1}$) were used. The equilibrium time for each run is 10 min.

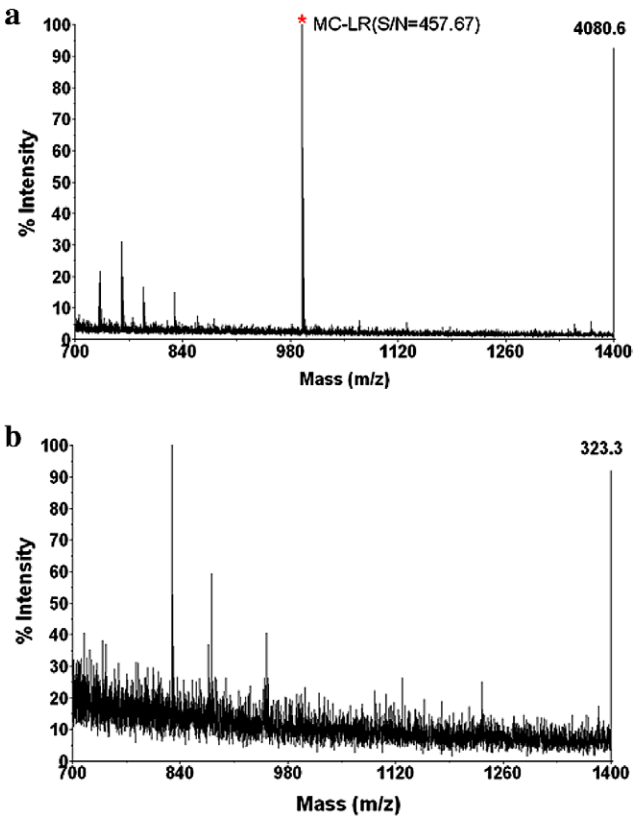


**Fig. 9.** MS spectra of MC-LR solution (200 μL, 10 μg/L) (a) before and (b) after treated by 0.6 mg of magnetic 3-D macroporous silica.

## 4. Conclusion

In this paper, a novel 3-D ordered macroporous magnetic-silica composite has been synthesized by a simple co-sedimentation of binary colloidal system of PMMA spheres and magnetite nanoparticles and infiltration of silica precursors. The obtained magnetic-silica composites pocess ordered macropore of ~200 nm with interconnected windows of about 50 nm, high magnetization (19.2 emu/g) and superparamagentism. By using them as absorbents, a fast and efficient removal of MC-LR with high removal efficiency (>93%) and removal capacity (3.3 ng MC/mg) can be achieved. Due to their ordered macroporous structure with large entrances and good affinity for biomacromolecules as well as high magnetization, our macroporous magnetic-silica composites may have great potential for various bio-related applications. The binary sedimentation method in this study can be extended to the synthesis of other functional ordered macroporous materials consisting of multicomponents, such as silica-metal nanoparticles, titania-Au nanoparticles and so on, which are important in catalysis, chemical sensors, optics and so on.

## Acknowledgments

This work was supported by NSF of China (20890123, 20721063, 20871030), State Key Basic Research Program of PRC (2006CB932302), Shanghai Leading Academic Discipline Project (B108), Shanghai Rising Star Program (08QA14010), Doctoral Program Foundation of State Education Commission of China (200802461013), and STCSM (08DZ2270500).

## References

[1] P. Lodahi, A.F. Driel, I.S. Nikolaev, A. Irman, K. Overgaag, D. Vanmaekelbergh, W.L. Vos, Nature 430 (2004) 654.
[2] (a) Y.H. Deng, D.W. Qi, C.H. Deng, X.M. Zhang, D.Y. Zhao, J. Am. Chem. Soc. 130 (2008) 28;
(b) L. Zhang, S.Z. Qiao, Y.G. Jin, Z.G. Chen, H.C. Gu, G.Q. Lu, Adv. Mater. 20 (2008) 805;
(c) L. Zhang, S.Z. Qiao, Y.G. Jin, H.G. Yang, S. Budihartono, F. Stahr, Z.F. Yan, X.L. Wang, Z.P. Hao, G.Q. Lu, Adv. Funct. Mater. 18 (2008) 3203.
[3] J. Llorca, A. Casanovas, T. Trifonov, A. Rodríguez, R. Alcubilla, J. Catal. 255 (2008) 228.
[4] A. Stein, F. Li, N.R. Denny, Chem. Mater. 20 (2008) 649.
[5] Z.Y. Wang, F. Li, N.S. Ergang, A. Stein, Chem. Mater. 18 (2006) 5543.
[6] P.M. Tessier, O.D. Velev, A.T. Kalambur, A.M. Lenhoff, J.F. Rabolt, E.W. Kaler, Adv. Mater. 13 (2001) 396.
[7] L. Lu, A. Eychmüller, Acc. Chem. Res. 41 (2008) 244.
[8] Y.N. Xia, G.M. Whitesides, Angew. Chem. Int. Edit. 37 (1998) 550.
[9] V.N. Manoharan, A. Imhof, J.D. Thorne, D.J. Pine, Adv. Mater. 13 (2001) 447.
[10] B.T. Holland, C.F. Blanford, A. Stein, Science 281 (1998) 538.
[11] Y.N. Xia, B. Gates, Z.Y. Li, Adv. Mater. 13 (2001) 409.
[12] D.J. Norris, Y.A. Vlasov, Adv. Mater. 13 (2001) 371.
[13] H. Míguez, F. Meseguer, C. López, F. López-Tejeira, J. Sanchez-Dehesa, Adv. Mater. 13 (2001) 393.
[14] .A. Imhof, D.J. Pine, Nature 389 (1997) 948.
[15] O.D. Velev, T.A. Jede, R.F. Lobo, A.M. Lenhoff, Nature 389 (1997) 447.
[16] O.D. Velev, E.W. Kaler, Adv. Mater. 12 (2000) 531.
[17] P.D. García, Á. Blanco, A. Shavel, N. Gaponik, A. Eychmüller, B. Rodríguez-González, L.M. Liz-Marzán, C. López, Adv. Mater. 18 (2006) 2768.
[18] Y.H. Deng, C. Liu, T. Yu, F. Liu, F.Q. Zhang, Y. Wan, L.J. Zhang, C.C. Wang, B. Tu, P.A. Webley, H.T. Wang, D.Y. Zhao, Chem. Mater. 19 (2007) 3271.
[19] Y.W. Jun, J.W. Seo, J. Cheon, Acc. Chem. Res. 41 (2007) 179.
[20] B. Gates, Y.N. Xia, Adv. Mater. 13 (2001) 1605.
[21] T. Sen, A. Sebastianelli, I.J. Bruce, J. Am. Chem. Soc. 128 (2006) 7130.
[22] T.S. Eagleton, P.C. Searson, Chem. Mater. 16 (2004) 5027.
[23] H.W. Yan, C.F. Blanford, B.T. Holland, M. Parent, W.H. Smyrl, A. Stein, Adv. Mater. 11 (1999) 1003.
[24] J. Galloro, M. Ginzburg, H. Miguez, S.M. Yang, N. Coombs, A. Safa-Sefat, J.E. Greedan, I. Manners, G.A. Ozin, Adv. Funct. Mater. 12 (2002) 382.
[25] Z.Z. Gu, H.H. Chen, S. Zhang, L.G. Sun, Z.Y. Xie, Y.Y. Ge, Colloid Surface A 302 (2007) 312.
[26] I. Nedkov, T. Merodiiska, L. Milenova, T. Koutzarova, J. Magn. Magn. Mater. 21 (2000) 296.
[27] V. Kitaev, G.A. Ozin, Adv. Mater. 15 (2003) 75.
[28] M.E. Leunissen, C.G. Christova, A.P. Hynninen, C.P. Royall, A.I. Campbell, A. Imhof, M. Dijkstra, R.V. Roij, A.V. Blaaderen, Nature 437 (2005) 235.
[29] Z.Y. Zhong, Y.D. Yin, B. Gates, Y.N. Xia, Adv. Mater. 12 (2000) 206.
[30] Y.H. Deng, C. Liu, D. Gu, T. Yu, B. Tu, D.Y. Zhao, J. Mater. Chem. 18 (2008) 91.
[31] Y. Chen, S.Z. Yu, Y.D. Lin, L. Hu, M. Xu, W. Shen, J.B. Yang, China Public Health 12 (2002) 1455.
[32] J. Lee, H.W. Walker, Environ. Sci. Technol. 40 (2006) 7336.
[33] P. Pendleton, R. Schumann, S.H. Wong, J. Colloid Interf. Sci. 240 (2001) 1.
[34] WHO, Cyanobacterial Toxins: Microcystin-LR Guidelines for Drinking Water Quality [M], second ed., World Health Organization, Geneva, 1998. pp. 95–110.